MALDI-2 on a trapped ion mobility quadrupole time-of-flight instrument for rapid mass spectrometry imaging and ion mobility separation of complex lipid profiles

Soltwisch, J.; Heijs, B.; Koch, A.; Vens-Cappell, S.; Hohndorf, J.; Dreisewerd, K.

analytical chemistry

pubs.acs.org/ac

Technical Note

MALDI-2 on a Trapped Ion Mobility Quadrupole Time-of-Flight Instrument for Rapid Mass Spectrometry Imaging and Ion Mobility Separation of Complex Lipid Profiles

Jens Soltwisch,[#] Bram Heijs,[#] Annika Koch, Simeon Vens-Cappell, Jens Höhndorf, and Klaus Dreisewerd*

Cite This: *Anal. Chem.* 2020, 92, 8697−8703

Read Online

ACCESS | Metrics & More | Article Recommendations | Supporting Information

ABSTRACT: Matrix-assisted laser desorption/ionization combined with laser-induced postionization (MALDI-2) is a recently introduced method for enhanced mass spectrometry imaging of numerous classes of biomolecules, including phospho- and glycolipids in tissue sections at high lateral resolution. Here we describe the first adaptation of the technology to a Bruker timsTOF fleX mass spectrometer. Upon use of a 1 kHz postionization laser, MALDI-2 produces a sizable increase in the number of detected features as well as in ion signal intensities. This enhancement is similar to that described previously for low repetition rate MALDI-2 systems, but now enables substantially enhanced measurement speeds. In our proof-of-concept study, we furthermore demonstrate, on examples of rat brain and testis tissue sections, that the combination of MALDI-2 with the trapped ion mobility spectrometry (TIMS) functionality of the instrument can crucially support unravelling the complex molecular composition of the lipidome. Numerous isomeric/isobaric ion species are successfully separated upon using the collisional cross section (CCS) as additional specific physical property. With the possibilities of high data acquisition speed or high separation powers in combination with the increased sensitivity of MALDI-2 available in one instrument, the described methodology could be a valuable tool in many areas of biological and medical research.

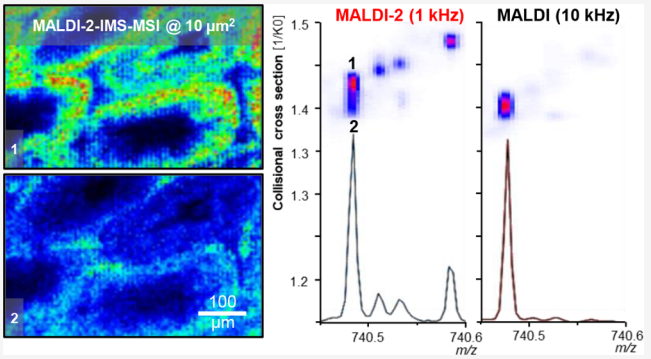

Matrix-assisted laser desorption/ionization time-of-flight mass spectrometry (MALDI-TOF-MS) is arguably the most widely used mass spectrometry imaging (MSI) technique for label-free visualization of the spatial distributions of numerous classes of biomolecules such as phospho- and glycolipids in thin tissue sections.[1] State of the art axial-TOF mass spectrometers provide fast data acquisition rates with routine pixel sizes of about 20 μm by cross section and, below, with carefully tuned methods.[2−4] However, with this instrument type, a confident assignment of the registered ions is restricted by a more limited mass resolving power and mass accuracy.[5] This problem is aggravated in the analysis of lipids, because the lipidome of most tissue types comprises several thousands of individual molecular species, with most lipid species being registered in a relatively small mass region between 300 and 900 Da. Many of these species exhibit molecular weights that differ only by small mass increments (i.e., they are isobaric) or constitute isomers.[6] In direct tissue analysis by MALDI-MSI, the absence of a molecular separation technique prior to desorption and ionization results in notorious ion suppression effects that greatly hamper the measurement sensitivity.[7−9] Consequently, a number of targeted methods to selectively increase ion yields for a specific class of analyte or deplete signal intensity of suppressors have been developed, such as on-tissue chemical derivatization or enzymatic digestion.[10−13]

In order to increase sensitivity for a number of heavily suppressed lipid classes in a less targeted way, we recently introduced a laser-based postionization (PI) strategy, named MALDI-2.[14] The mechanisms underlying MALDI-2 are still under discussion.[15,16] In the prevailing proposed mechanism, a second Q-switched laser pulse with a UV wavelength below the two-photon ionization threshold of the matrix intersects the expanding MALDI-plume at a short distance above the sample (~500 μm). Resonance-enhanced two-photon ionization of the aromatic matrix molecules leads to the production of high abundances of additional matrix ions. Concurrently, the evolving MALDI plume is decelerated and confined by a

Received: April 23, 2020
Accepted: May 24, 2020
Published: May 24, 2020

https://dx.doi.org/10.1021/acs.analchem.0c01747
Anal. Chem. 2020, 92, 8697−8703

background pressure between 2 and 10 mbar (0.2−1 kPa), forming what is essentially a temporary gas-phase reaction vessel. In this vessel, charges transfer from the postionized matrix to neutral analyte molecules in a multitude of secondary reactions, in particular, via proton transfer.[14] In effect, this cascade of chemical reactions can boost the ion yields for numerous analyte classes (e.g., phospho- and glycolipids, secondary metabolites, pharmaceuticals, and oligosaccharides) by up to 2−3 orders of magnitude and both ion modes.[17−19]

So far, MALDI-2 has been implemented on platforms with relatively low laser repetition rates (Synapt G2-S QTOF; Waters/Micromass, Manchester, U.K.; 20 Hz laser repetition rate (measurement speed: 1−5 pixels/s)[9,14] and different orbital trap mass spectrometers (Thermo Fisher Scientific, Bremen, Germany; 60 and 100 Hz laser repetition rate (measurement speed: 1−5 pixel/s));[17−22] in the latter cases, a dual ion funnel MALDI/ESI source from Spectroglyph (Kennewick, WA) was consistently used.

With a larger portion of the lipidome now accessible by MALDI-2-MSI, the mass spectra inevitably become more complex, and the separation and identification of isobaric lipid species becomes increasingly challenging. One approach to improve this situation for all nonisomeric species is the use of high resolution, accurate mass (HRAM) mass spectrometers, such as Fourier-transform (FT) based-ion trap instruments (orbitrap and FT-ICR, where ICR stands for ion cyclotron resonance).[17,23,24] However, with these instruments generally only low data acquisition rates are possible.

Another way to enhance the number of molecular identifications in MALDI-MSI is by applying ion mobility separation (IMS).[7,25,26] Available through different technical realizations, IMS is typically interposed between ion source and mass analyzer and results in the spatiotemporal separation of ions based on their collisional cross section (CCS) prior to m/z-based separation and detection.[27,28] IMS-MS has helped to decipher molecular confirmation in proteomics applications and has developed into a very powerful tool in structural analysis, especially for peptides and lipids.[29−34] MALDI-IMS-MSI has also been successfully combined with a laser postionization approach in the spatially resolved analysis of noncovalently bound peptide complexes.[35]

Recently, Bruker amended their electrospray ionization trapped ion mobility mass spectrometer (ESI-TIMS-QTOF-MS) with a dual MALDI-ESI source, marketed under the trade name timsTOF fleX. With this setup and using shotgun ESI-MS as well as MALDI-MSI, it was recently demonstrated that the combination of high mass accuracy and IMS separation serves as an exquisite tool for separation and identification in the analysis of complex lipid mixtures.[7,34] Here we introduce the first adaptation of MALDI-2 on a timsTOF fleX mass spectrometer and show how the use of a 1 kHz postionization laser enables data acquisition rates of up to 33 pixel/s using suited methods. In proof-of-concept experiments, we furthermore demonstrate how the use of MALDI-2-IMS-MSI substantially increases the number of distinct features that can potentially be assigned when analyzing the intensity surface spanned by m/z and mobility-values, or 2D mobility plot, as compared to peak picking in the mass spectrometric dimension alone.

EXPERIMENTAL SECTION

A detailed description of chemicals and methods used in sample preparation as well as data analysis is provided in the Supporting Information (SI).

MALDI-2 Modifications to the timsTOF fleX. All mass spectrometric measurements where performed on a modified timsTOF fleX instrument. The mobility resolution (Ω) is about 200 and the mass resolving power R of the QTOF-type instrument is typically 40000 (fwhm) in the lipid mass range, providing a mass accuracy of better than 2 ppm with external calibration. The Bruker SmartBeam 3D Laser (an actively Q-switched, frequency-tripled diode-pumped solid state laser emitting at 355 nm) allows rapid MALDI-MS image acquisition at rates up to 15 pixels/s in standard MALDI-QTOF operation. Modifications to the prototype instrument allowed to minimize the influence of stage movement on measurement time in order to investigate the influence of laser repetition rate on this parameter under optimal conditions. It should be noted that under these "high-speed" conditions pixel fidelity can be compromised, leading to distortions and discontinuities in the resulting images.

Two CaF_2 vacuum windows were added to the MALDI ion source and the beam of a diode-pumped, actively Q-switched, frequency-quadrupled Nd:YAG laser (NL 204-1k-FH, EKSPLA, Vilnius, Lithuania; wavelength, 266 nm; pulse duration, 7 ns; maximal pulse repetition rate, 1 kHz; maximum pulse energy, ∼500 μJ) was aligned parallel to the plane of the sample surface. A beam dump (10BD02, Standa, Vilnius, Lithuania) served for absorbing the beam at the exit side of the chamber. Prior to being introduced into the ion source, the PI laser beam was expanded 3-fold using a telescope consisting of plano-convex CaF_2 lenses with focal lengths of 50 and 150 mm, and a diameter of 25 mm, each. A third plano-convex CaF_2 lens with a focal length of 600 mm and 25 mm diameter served to focus the beam to a position centrally located above the MALDI laser ablation site. The beam waist of the focused PI laser was about 85 μm wide, as determined by inspection of burn holes in paper. The central distance of the PI laser beam to the sample surface was adjusted to about 500 μm using a set of manual optomechanic mirror mounds and dielectrically coated mirrors. The laser pulse energy was adjusted by attenuating the pumping diode current. All windows, lenses, and mirrors were purchased from Edmund Optics (Mainz, Germany).

Key to MALDI-2 experiments is a precise synchronization of the two laser pulses relative to each other, to electronics of the mass spectrometer, and the data acquisition. For conventional MALDI and material ablation in the MALDI-2 experiments, the SmartBeam 3D laser of the timsTOF fleX was used. The maximum repetition rate of the SmartBeam 3D laser is 10 kHz, but for MALDI-2 experiments it was limited to 1 kHz to allow synchronization to the PI laser. For synchronization, a trigger derived by the instrument's electronics was fed into a pulse delay generator (Quantum Composer 9214, Schulz Electronic, Baden−Baden, Germany; jitter: <0.5 ns), processed, and used to trigger the PI laser. The Q-Switch trigger signal (SmartBeam 3D) as well as a fast photo diode, read out by an oscilloscope (PI-laser), were used to measure and control the interlaser pulse delay time.

Guided by previous fundamental MALDI-2 studies,[37] the optimum value for the PI laser energy was identified to ∼200 μJ, the interlaser pulse delay time to 10 μs, and the N_2 buffer

https://dx.doi.org/10.1021/acs.analchem.0c01747
Anal. Chem. 2020, 92, 8697−8703

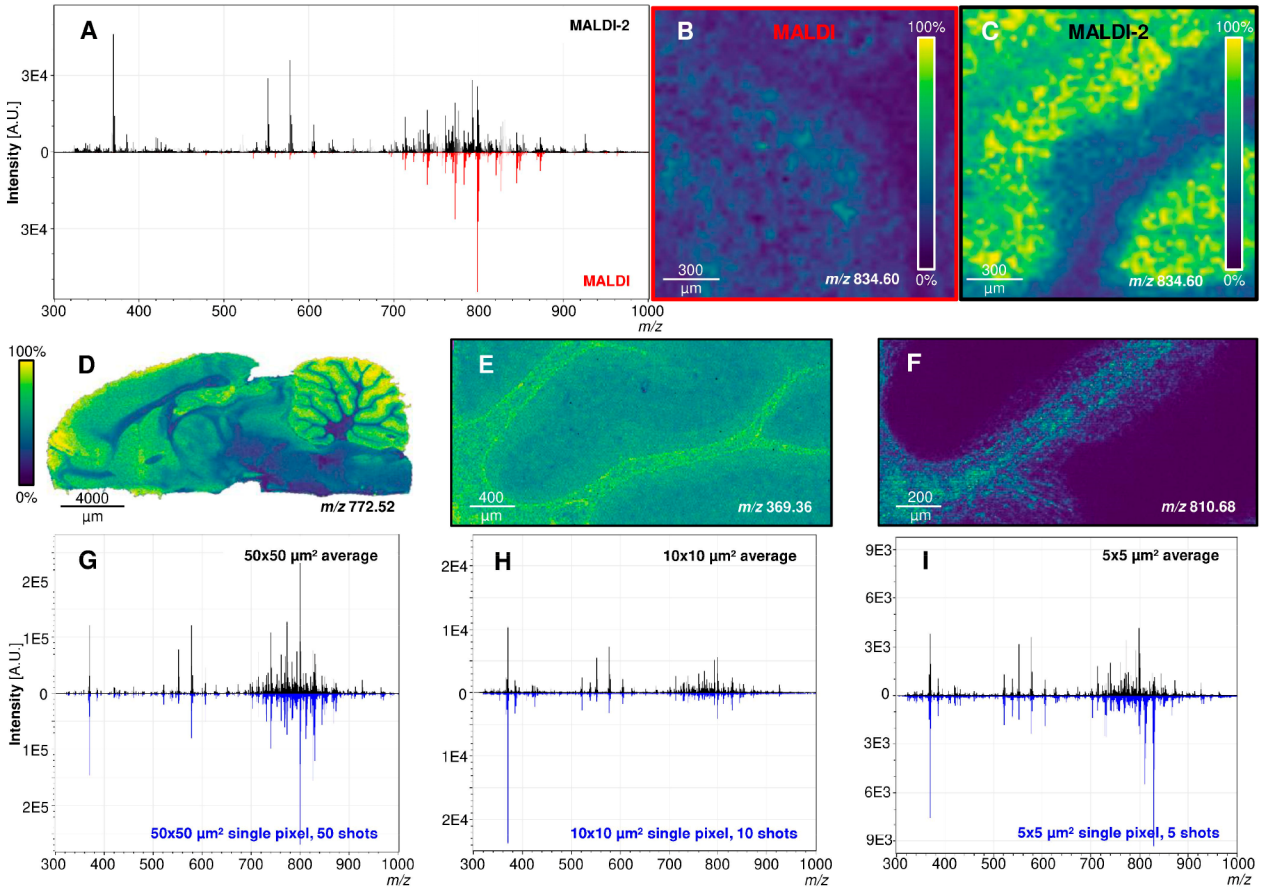

Figure 1. Overview of timsTOF fleX MALDI-2-MSI data of lipids registered from rat brain sections. (A) Average mass spectra of MALDI-2-MSI (top, black trace) and MALDI-MSI (bottom, red trace) analyses of rat cerebellum. The MALDI data set consists of 40249 pixels and was recorded at 22 pixels/s using a 10 kHz laser repetition rate and 20 shots/pixel. The MALDI-2 data set consists of 46818 pixels and was recorded at 16 pixels/s using a 1 kHz laser repetition rate and 20 shots/pixel. Ion distribution of m/z 834.60 (PC(40:6) $[M + H]^+$) in (B) the MALDI and (C) MALDI-2 analyses, respectively. (D−F) Additional lipid distributions revealed by the MALDI-2-MSI analyses: (D) m/z 772.52 (PC(32:0) $[M + K]^+$) at 50 × 50 μm^2, recorded using the "M5 small" laser setting, 1 kHz laser repetition rate, and 50 shots/pixel (15 pixels/s); (E) m/z 369.36 (cholesterol−H_2O $[M + H]^+$) at 10 × 10 μm^2, recorded using the "single" laser setting with "beam scan", 1 kHz laser repetition rate, and 10 shots/pixel (33 pixels/s); (F) m/z 810.68 (HexCer(d18:1/C24:1) $[M + H]^+$) at 5 × 5 μm^2, recorded using the "single" laser setting without "beam scan", 1 kHz laser repetition rate, and 5 shots/pixel (33 pixels/s); we note that based on the data, we cannot decide on the presence of isomeric lipoforms of this glycosphinolipid (e.g., comprising a galactose versus glucose moiety) and that of varying combinations in the ceramide part (e.g., (d20:1/C22:1). In (G)−(I), the respective average (black) and single white-matter pixel (blue) mass spectra for the datasets recorded in (D)−(F). All images are displayed after RMS normalization, equivalent non-normalized images can be found in Figure S-4 (SI), and tandem MS spectra of the identified lipid species can be found in Figure S-5.

gas pressure in the region of ion generation to ∼2.6 mbar (260 Pa). When engaged, TIMS separation (1/K0-range 1.10−1.70) was performed using N_2 as collision gas, a ramp time of 800 ms, and a duty cycle of 25% (200 shots/pixel). Prior to all analyses, the QTOF mass analyzer as well as the TIMS separation were calibrated using the ESI-L low molecular weight tunemix.

Laser Irradiation Parameters. For the initial MALDI event, a SmartBeam 3D laser system with galvanometric scanning was used for all experiments.[2] The laser beam with a Gaussian beam profile is focused onto the sample surface at 35° to the surface normal and produces an ablation mark of about 5 μm by diameter, as determined by light microscopy. Note that for Gaussian beams ablation size of ablation marks may change with laser pulse energy and matrix material and thickness. To produce the circular 5 μm pixel the Gaussian laser spot was not scanned and used stationary. With 10 × 10 μm^2 and 20 × 20 μm^2 pixels, the full area was ablated by scanning the 5 μm wide laser spot over the full pixel area, which resulted in a near square ablation mark as described before.[2] For the largest tested pixel size of 50 × 50 μm^2 the "M5 small" option was used. Described in detail elsewhere,[38] this setup splits up the Gaussian laser beam into five separate beams that are simultaneously focused onto the sample in the pattern of the five on a dice. In combination with beam scanning the pattern of all five beams in parallel, a pixel size of 50 × 50 μm^2, therefore, consists of five irradiated (each 16 × 16 μm^2) and four nonirradiated near-squares, arranged in a checkerboard pattern.

RESULTS AND DISCUSSION

Increased Sensitivity by MALDI-2. As demonstrated by Figures 1 and 2, the use of the PI laser leads to a strong increase of the total number of features registered from the investigated brain and testis sections as well as signal intensities of individual ion species in the investigated mass range (m/z 300−1000) (Figure S-1A, SI). This includes matrix as well as

https://dx.doi.org/10.1021/acs.analchem.0c01747
Anal. Chem. 2020, 92, 8697−8703

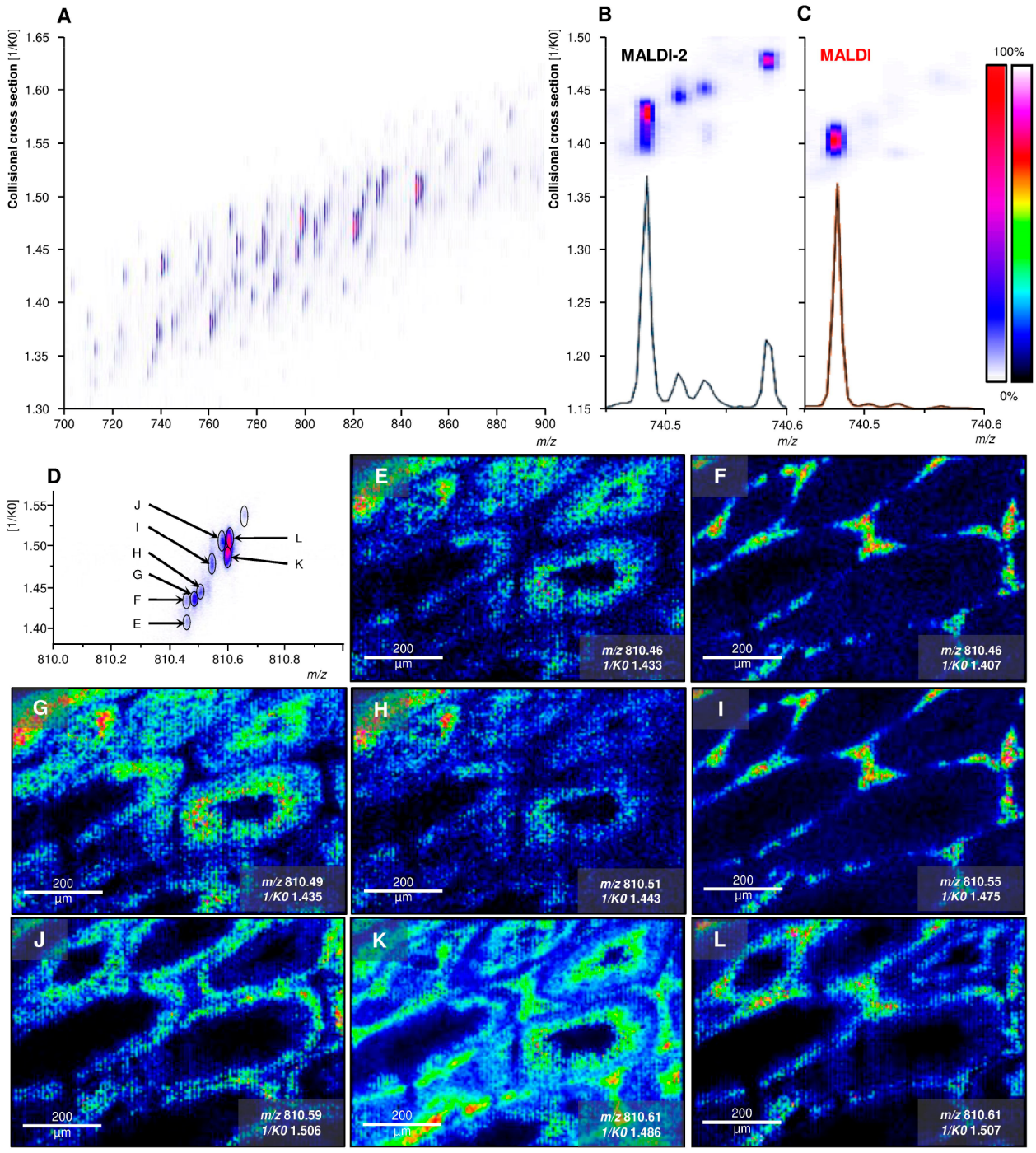

Figure 2. MALDI-2-IMS-MSI of lipids in rat testis. (A) 2D-mobility plot of the phospholipid region recorded with MALDI-2. The data set consisted of 20838 10 × 10 μm^2 pixels and was recorded using a "ramp time" of 800 ms between 1/K0 1.10−1.70. A comparison between (B) MALDI-2 and (C) MALDI analyses was performed, clearly showing the wealth of additional features gained in the MALDI-2 analysis. (D) The *m/z*-region 810.0−811.0, displaying nine distinct features, of which the distributions of eight in the testis section are visualized in the ion images of (E)−(L). The *m/z*-intensity representation of (D) can be found in Figure S2-A (SI). Note that the features (E, F and J−L) were only separated by using TIMS and contribute to the same *m/z*-feature. All images are displayed without normalization.

analyte ion species and possible in-source decay (ISD) fragments and adducts. While no additional ISD of lipids has been observed for MALDI-2, a signal intensity increase of fragment ions can be explained with increasing ionization efficiencies for these ions in MALDI-2.[22,36] On average, the number of peaks detected by MALDI-2 from a sagittal rat brain section was 40% higher compared to conventional MALDI when a signal-to-noise (S/N) ratio ≥20 was set as peak picking criterion (Figure S-1B, SI). Peak picking with a relative intensity threshold of 0.5% resulted in an increase of the average detected number of peaks in MALDI-2 by 76%. These results are in full agreement with the previously reported MALDI-2 studies.[14,17−22] Also in line with the previous work, major MALDI-2-derived ions are predominantly comprising

https://dx.doi.org/10.1021/acs.analchem.0c01747
Anal. Chem. 2020, 92, 8697−8703

$[M + H]^+$ species in the positive ion mode and deprotonated molecules $[M - H]^-$ in the negative ion mode (data not shown). As observed in earlier studies on QTOF type instruments, signal intensities of $[M + Na]^+$ and $[M + K]^+$ ions are only slightly increased or remain largely unchanged. A more comprehensive assignment was beyond the scope of this technical note but will be included in follow-up application-driven studies.

Combination of MALDI-2 with TIMS for Increased Feature Recognition. Based on a $S/N > 20$, around 600 peaks were discerned in the average spectra after conventional MALDI (Figure S-1A, SI). For MALDI-2, this number was between 1000 and 1500, depending on the pixel size used for the analysis. Next to a sizable share of matrix-related peaks, it can be assumed that a large portion of these peaks is related to a wide variety of lipid species. However, as demonstrated recently by Bowman et al. using ultrahigh resolving power MALDI-MSI, the presence of ion species with m/z-values varying by ≤10 mDa are more the rule than the exception in the MALDI-MSI analysis of this "lipid mass range".[24] With the mass resolving power available on timsTOF fleX of 40000 in the lipid region, consequently, this leads to a substantial number of isobaric species that remain unresolved in the m/z-domain.

Figure 2 demonstrates how IMS can be used as an additional dimension of molecular separation to resolve isobaric and isomeric lipid ion species, tightly packed in the m/z-domain. Specifically, Figure 2A shows an overview of the 2D-mobility plot of the m/z-region between 700 and 900 from a MALDI-2-IMS-MSI measurement of rat testis. The apparent cloud shaped arrangement of features, as opposed to a thin line, indicates a successful separation of (near)-isobaric ion species. As depicted in Figure 2B,C, this advantage becomes increasingly valuable in combination with MALDI-2, where signal intensity for a sizable number of additional ion species is significantly increased. Whereas a single peak dominates the depicted 2D space in the conventional MALDI mass spectrum, four to five additional features were clearly discerned using MALDI-2 with additional features near the S/N threshold. To demonstrate the benefit gained by a 2D-feature analysis for MALDI-2 data, Figure 2D shows the 2D mobility plot region of lipid species with m/z values between 810.0 and 811.0. Within this narrow m/z window, nine features are separated. For eight of these features their distribution in the tissue is depicted in Figure 2E−L. In contrast, only five peaks can be detected by m/z analysis alone (Figure S-2A, SI). Notably, a pair of true isobars (Figure 2E,F) and a cluster of three near-isobaric species (Figure 2J−L) were separated in this small m/z window alone. For both groups of ion species, an image constructed based on m/z alone essentially produced an intensity distribution that was similar to the overlay of the signal intensities of the IMS-separated ion species (Figure S-2B, C, SI). The additional TIMS measurement with suitable resolving power comes at the cost of decreased measurement speed. A ramp time of 800 ms, as used in the presented data, for example, resulted in a data acquisition speed of 1.2 pixels/s (compared to 33 pixel/s with IMS disabled). Also, depending on the desired resolving power of the IMS, the accessible mass range may be limited.

Comparing the Data Acquisition Speeds of MALDI and MALDI-2-MSI at Different Pixel Sizes. Figure 1 summarizes, at the example of a sagittal section of rat brain, the performance of MALDI-2-MSI (without IMS) at 1 kHz laser pulse repetition rate for different pixel sizes and compares it to the performance of conventional MALDI-MSI at the maximum available pulse repetition rate of 10 kHz. Four different settings for focusing of the MALDI laser were tested ranging from pixel sizes from 5 μm by diameter (stationary round Gaussian beam) to fully irradiated pixels 10×10 μm^2 and 20×20 μm^2 (beam scanning) and to approximately 50×50 μm^2 pixels of a checkerboard-type footprint (beam splitting and scanning).

To assess the effect of the laser repetition rate on measurement speed, specific methods were optimized to ensure maximized pixel-to-pixel speed. These changes helped to minimize the influence of stage movement on scan speed in order to expose the influence of laser repetition rate as much as possible. As mentioned above, these changes come at the cost of a compromised pixel fidelity and are not advised for regular imaging experiments. Under slightly slower standard conditions, where high pixel fidelity and therefore high image quality are maintained, differences between 1 and 10 kHz can be expected to be of less influence than described below. It should be carefully noted that, in the measurement speed calculations, additional features contributing to total acquisition time (e.g., fly back time) were excluded. At the available high pulse repetition rates of 1 kHz (MALDI-2) and 10 kHz (MALDI) fast measurement speeds, between 16 and 33 pixels/s, were available for both "high-speed" methods. In a direct comparison, with the number of laser shots per pixel fixed, at a pixel size of 50×50 μm^2, MALDI-MSI at 10 kHz repetition rate had a measurement speed twice as fast as its MALDI-2 counterpart at 1 kHz, albeit in total a lower molecular coverage is obtained. It should be noted that, for the 50×50 μm^2 measurements, the average acquisition-time-per-pixel (influenced by total number of pixels, fly backs, etc.) was approximately four times shorter in MALDI (0.038 s/pixel), compared to MALDI-2 (0.147 s/pixel). At smaller pixel sizes ($\leq 10 \times 10$ μm^2) and a reduced number of laser shots per pixel, the differences in both measurement speed and acquisition-time-per-pixel between MALDI and MALDI-2 were ≤10%, while maintaining high quality single-pixel spectra (Supplemental Methods, Figure S-3 and Table S-1, SI).

Figure 1B,C shows the effect of the increase in signal intensity at the example images of the ion recorded at m/z 834.60 (identified by tandem MS as $[PC(40:6) + H]^+$, Figure S-5, SI); the images were acquired at a pixel size of 20×20 μm^2. An even stronger increase in sensitivity was observed for members of lipid classes that suffer particularly strongly from ion suppression effects such as phosphatidylethanolamine or neutral glycosphingolipids, where ion signals in normal MALDI mode are often close to or below the limit of detection. For example, MALDI-2 boosted the $[M + H]^+$ ion yields for hexosylceramide HexCer(d18:1/C24:1) to the extent that single-pixel tandem MS provided high quality and informative structural information, allowing in situ structure elucidation (Figure S-5D, SI). To investigate the influence of the laser profile and ablation area on the efficiency of MALDI-2, we employed three additional pixel sizes, 50×50 μm^2, 10×10 μm^2, and 5 μm diameter, as described in the SI. Generated mass spectra from the scanning (Figure 1A,H) and non-scanning (Figure 1I) Gaussian beam irradiation show great similarities with overall signal intensity, decreasing with spot size, as expected. Even at the smallest pixel size, single pixel spectra were still rich in information with sufficient overall S/N ratio (Figure 1I). The MALDI-2 spectrum generated with the 50×50 μm^2 setting produced the overall highest signal

https://dx.doi.org/10.1021/acs.analchem.0c01747
Anal. Chem. 2020, 92, 8697−8703

intensity and a comparable profile to the pixel sizes where the full pixel area was ablated (Figure 1G). For all stationary single beam experiments and beam scanning, laser parameters were set to produce ablation marks of about 5 μm on unperturbed matrix preparation. Results for these experiments were in good agreement with the previously reported influence of the laser spot size on the optimal interlaser pulse delay time, as well as the overall efficiency of the MALDI-2 process.[37] In case of laser beam splitting (Figure 1G), beneficial effects by MALDI-2 in terms of an increase in signal intensity as well as the number of detectable peaks are somewhat less-pronounced. It may be speculated that the change in laser profile may lead to changes in plume formation and, therefore, requires adjustments in interlaser pulse delay for optimal MALDI-2 performance.[37,38] The images produced at the different settings obviously improve in quality toward smaller pixel sizes. It is important to note that the dynamic range is maintained over the array of pixel sizes, resulting in good contrast between different morphological areas in the tissues (Figure 1C–F).

CONCLUSIONS

In conclusion, the combination of MALDI-2 with ion mobility separation on a timsTOF fleX instrument harbors great potential for the MSI analysis of lipids and, though not tested in this study, presumably for further classes of biomolecules. For all employed pixel sizes between 5 × 5 and 50 × 50 μm^2 MALDI-2 produced a sizable increase in overall signal intensity, as well as the number of detectable peaks in the mass spectra. Whereas the development of dedicated software to handle IMS-MSI data is currently still pending, our data show that feature finding in the 2D-m/z ion mobility domain instead of the m/z-domain alone will not only enable a substantial increase in the number of recognized features, but also deliver a second independent variable describing each feature. Database searches based on two variables, m/z and CCS (instead of m/z alone), will thus allow for a more confident assignment of molecular identities. Our data moreover demonstrates the applicability of the MALDI-2 technique to high repetition rates of 1 kHz for stationary ablation, as well as ablation with beam scanning, beam splitting, and a combination of the latter, used during the initial MALDI event. This makes the technique highly compatible with sophisticated laser systems and high acquisition speeds of modern MALDI-MSI platforms.

ASSOCIATED CONTENT

Supporting Information

The Supporting Information is available free of charge at https://pubs.acs.org/doi/10.1021/acs.analchem.0c01747.

Additional methods on sample preparation, and MALDI and MALDI-2 speed calculations; Images of simulated MALDI-2-MSI data from the MALDI-2-IMS-MSI data; MALDI stage speeds at various pixel sizes and irradiation parameters; Non-normalized MALDI-2-MSI images of lipid distributions at various pixel sizes in rat brain; Tandem MS spectra of the identified lipid species; Tables with measurement speed and acquisition times for MALDI and MALDI-2 at various pixel sizes (PDF)

AUTHOR INFORMATION

Corresponding Author

Klaus Dreisewerd − *Institute of Hygiene and Interdisciplinary Center for Clinical Research (IZKF), University of Münster, 48149 Münster, Germany;* orcid.org/0000-0002-7619-808X; Email: dreisew@uni-muenster.de

Authors

Jens Soltwisch − *Institute of Hygiene and Interdisciplinary Center for Clinical Research (IZKF), University of Münster, 48149 Münster, Germany;* orcid.org/0000-0002-0258-1561

Bram Heijs − *Institute of Hygiene, University of Münster, 48149 Münster, Germany; Center for Proteomics and Metabolomics, Leiden University Medical Center, 2333 ZA Leiden, The Netherlands*

Annika Koch − *Bruker Daltonik GmbH, 28359 Bremen, Germany*

Simeon Vens-Cappell − *Bruker Daltonik GmbH, 28359 Bremen, Germany*

Jens Höhndorf − *Bruker Daltonik GmbH, 28359 Bremen, Germany*

Complete contact information is available at: https://pubs.acs.org/10.1021/acs.analchem.0c01747

Author Contributions

#These authors contributed equally to this work. They are both first authors.

Notes

The authors declare the following competing financial interest(s): Annika Koch, Simeon Vens-Cappell, and Jens Höhndorf are employees of Bruker Daltonik GmbH (Bremen); Bram Heijs has been supported by Bruker Daltonik during the cause of the project. All other authors declare no conflict of interest.

ACKNOWLEDGMENTS

The authors thank Andreas Haase and Henning Peise (both Bruker) for their valuable contributions in designing and modifying the MALDI-2-timsTOF fleX instrument. Financial support by the German Research Foundation (DFG; Grants DR416/12-1 and SO976/3-1, Project Number 290343045, to K.D. and J.S.; SO976/5-1, Project Number 400912714, to J.S.) and the Interdisciplinary Center for Clinical Research (IZKF) of the Münster University Medical School (Grant Drei2/018/17, to K.D. and J.S.) is gratefully acknowledged.

REFERENCES

(1) Buchberger, A. R.; DeLaney, K.; Johnson, J.; Li, L. *Anal. Chem.* **2018**, *90* (1), 240−265.

(2) Potočnik, N. O.; Porta, T.; Becker, M.; Heeren, R. M. A.; Ellis, S. R. *Rapid Commun. Mass Spectrom.* **2015**, *29* (23), 2195−2203.

(3) Ellis, S. R.; Cappell, J.; Potočnik, N. O.; Balluff, B.; Hamaide, J.; van der Linden, A.; Heeren, R. M. A. *Analyst* **2016**, *141*, 3832−3841.

(4) Kurabe, N.; Igarashi, H.; Ohnishi, I.; Tajima, S.; Inoue, Y.; Takahashi, Y.; Setou, M.; Sugimura, H. *World J. Gastrointest. Pathophysiol.* **2016**, *7* (2), 235−241.

(5) Palmer, A.; Phapale, P.; Chernyavsky, I.; Lavigne, R.; Fay, D.; Tarasov, A.; Kovalev, V.; Fuchser, J.; Nikolenko, S.; Pineau, C.; Becker, M.; Alexandrov, T. *Nat. Methods* **2017**, *14* (1), 57−60.

(6) Blanksby, S. J.; Mitchell, T. W. *Annu. Rev. Anal. Chem.* **2010**, *3*, 433−465.

(7) Spraggins, J. M.; Djambazova, K. V.; Rivera, E. S.; Migas, L. G.; Neumann, E. K.; Fuetterer, A.; Suetering, J.; Goedecke, N.; Ly, A.;

van de Plas, R.; Caprioli, R. M. *Anal. Chem.* **2019**, *91* (22), 14552−14560.
(8) Perry, W. J.; Patterson, N. H.; Prentice, B. M.; Neumann, E. K.; Caprioli, R. M.; Spraggins, J. M. *J. Mass Spectrom.* **2020**, *55*, No. e4491.
(9) Boskamp, M. S.; Soltwisch, J. *Anal. Chem.* **2020**, *92* (7), 5222−5230.
(10) Amoscato, A. A.; Sparvero, L. J.; He, R. R.; Watkins, S.; Bayir, H.; Kagan, V. E. *Anal. Chem.* **2014**, *86* (13), 6587−6595.
(11) Wu, Q.; Comi, T. J.; Li, B.; Rubakhin, S. S.; Sweedler, J. V. *Anal. Chem.* **2016**, *88* (11), 5988−5995.
(12) Vens-Cappell, S.; Kouzel, I. U.; Kettling, H.; Soltwisch, J.; Bauwens, A.; Porubsky, S.; Müthing, J.; Dreisewerd, K. *Anal. Chem.* **2016**, *88* (11), 5595−5599.
(13) Wang, S.-S.; Wang, Y.-J.; Zhang, J.; Sun, T.-Q.; Guo, Y.-L. *Anal. Chem.* **2019**, *91* (6), 4070−4076.
(14) Soltwisch, J.; Kettling, H.; Vens-Cappell, S.; Wiegelmann, M.; Müthing, J.; Dreisewerd, K. *Science* **2015**, *348* (6231), 211−215.
(15) Huang, F.; Fan, X.; Murray, K. K. *Int. J. Mass Spectrom.* **2008**, *274* (1−3), 21−24.
(16) Potthoff, A.; Dreisewerd, K.; Soltwisch, J. Detailed characterization of the post-ionization efficiencies in MALDI-2 as a function of relevant input parameters. *J. Am. Soc. Mass Spectrom.* **2020**, under revision; not yet published.
(17) Ellis, S. R.; Soltwisch, J.; Paine, M. R. L.; Dreisewerd, K.; Heeren, R. M. A. *Chem. Commun.* **2017**, *53*, 7246−7249.
(18) Barré, F. P. Y.; Paine, M. R. L.; Flinders, B.; Trevitt, A. J.; Kelly, P. D.; Ait-Belkacem, R.; Garcia, J. P.; Creemers, L. B.; Stauber, J.; Vreeken, R. J.; Cillero-Pastor, B.; Ellis, S. R.; Heeren, R. M. A. *Anal. Chem.* **2019**, *91* (16), 10840−10848.
(19) Bowman, A. P.; Bogie, J. F. J.; Hendriks, J. J. A.; Haidar, M.; Belov, M.; Heeren, R. M. A.; Ellis, S. R. *Anal. Bioanal. Chem.* **2020**, *412*, 2277−2289.
(20) Bednařík, A.; Bölsker, S.; Soltwisch, J.; Dreisewerd, K. *Angew. Chem., Int. Ed.* **2018**, *57* (37), 12092−12096.
(21) Spivey, E. C.; McMillen, J. C.; Ryan, D. J.; Spraggins, J. M.; Caprioli, R. M. *J. Mass Spectrom.* **2019**, *54* (4), 366−370.
(22) Niehaus, M.; Soltwisch, J.; Belov, M. E.; Dreisewerd, K. *Nat. Methods* **2019**, *16*, 925−931.
(23) Römpp, A.; Spengler, B. *Histochem. Cell Biol.* **2013**, *139*, 759−783.
(24) Bowman, A. P.; Blakney, G. T.; Hendrickson, C. L.; Ellis, S. R.; Heeren, R. M. A.; Smith, D. F. *Anal. Chem.* **2020**, *92* (4), 3133−3142.
(25) Jackson, S. N.; Ugarov, M.; Egan, T.; Post, J. D.; Langlais, D.; Schultz, J. A.; Woods, A. S. *J. Mass Spectrom.* **2007**, *42* (8), 1093−1098.
(26) Barré, F.; Rocha, B.; Dewez, F.; Towers, M.; Murray, P.; Claude, E.; Cillero-Pastor, B.; Heeren, R. M. A.; Porta Siegel, T. *Int. J. Mass Spectrom.* **2019**, *437*, 38−48.
(27) Hopfgartner, G. *Anal. Bioanal. Chem.* **2019**, *411*, 6227.
(28) Dodds, J. N.; Baker, E. S. *J. Am. Soc. Mass Spectrom.* **2019**, *30* (11), 2185−2195.
(29) Sharon, M.; Robinson, C. V. *Annu. Rev. Biochem.* **2007**, *76*, 167−193.
(30) Stauber, J.; MacAleese, L.; Franck, J.; Claude, E.; Snel, M.; Kaletas, B. K.; Wiel, I. M. V. D.; Wisztorski, M.; Fournier, I.; Heeren, R. M. A. *J. Am. Soc. Mass Spectrom.* **2010**, *21* (3), 338−347.
(31) Shvartsburg, A. A.; Isaac, G.; Leveque, N.; Smith, R. D.; Metz, T. O. *J. Am. Soc. Mass Spectrom.* **2011**, *22* (7), 1146−1155.
(32) Cole, L. M.; Mahmoud, K.; Haywood-Small, S.; Tozer, G. M.; Smith, D. P.; Clench, M. R. *Rapid Commun. Mass Spectrom.* **2013**, *27* (21), 2355−2362.
(33) Meier, F.; Beck, S.; Grassl, N.; Lubeck, M.; Park, M. A.; Raether, O.; Mann, M. *J. Proteome Res.* **2015**, *14* (12), 5378−5387.
(34) Vasilopoulou, C. G.; Sulek, K.; Brunner, A.-D.; Meitei, N. S.; Schweiger-Hufnagel, U.; Meyer, S. W.; Barsch, A.; Mann, M.; Meier, F. *Nat. Commun.* **2020**, *11* (1), 331.
(35) Woods, A. S.; Jackson, S. N.; Lewis, E. K.; Egan, T.; Muller, L.; Tabet, J.-C.; Schultz, J. A. *J. Proteome Res.* **2013**, *12* (4), 1668−1677.
(36) Fuchs, B.; Bischoff, A.; Süß, R.; Teuber, K.; Schürenberg, M.; Suckau, D.; Schiller, J. *Anal. Bioanal. Chem.* **2009**, *395*, 2479.
(37) Niehaus, M.; Soltwisch, J. *Sci. Rep.* **2018**, *8*, 7755.
(38) Holle, A.; Haase, A.; Kayser, M.; Höhndorf, J. *J. Mass Spectrom.* **2006**, *41* (6), 705−716.

https://dx.doi.org/10.1021/acs.analchem.0c01747
Anal. Chem. 2020, 92, 8697−8703